An Atmospheric Solitary Gust Observed with a Doppler Radar, a Tall Tower and a Surface Network

RICHARD J. DOVIAK AND RUNSHENG GE[1]

National Severe Storms Laboratory, NOAA, Norman, OK 73069

(Manuscript received 24 January 1983, in final form 19 June 1984)

ABSTRACT

Doppler radar and a 444 m tall instrumented tower provide a detailed view of the kinematic and thermodynamic structure of a solitary gust. A study of the data fields, and comparison with theoretical and laboratory work leads to the conclusion that the gust is an internal solitary wave of permanent form launched by a thunderstorm outflow onto an inversion layer formed by the passage of an earlier storm. Comparisons with results from fluid experiments and numerical models are made and the similarities are striking. Both observations show turbulent breakdown at the rear of the wave. The ease with which solitary waves can be generated in experiments gives reason to believe that these nonlinear waves might be of considerable interest in the context of geophysical fluid dynamics.

1. Introduction

In the late evening of 11 May 1980, a solitary gust propagated 100 km from its thunderstorm source to be observed by NSSL's Doppler weather radar, a 444 meter tall meteorologically instrumented television tower, and by a surface network of automated weather stations all yielding unique data on this long lasting ($\geq 1\frac{1}{2}$ h) phenomenon. A survey of gust front data for the 15 April–15 June 1980 and 1981 seasons in Central Oklahoma showed that, of the ten gust events observed by Doppler radar, there were simultaneous tall tower data for only the one case reported herein. Although the radar has the advantage of surveying vast areas of the boundary layer in order to observe winds in many solitary gusts, the tower is an invaluable source of detailed thermodynamic information on these phenomena. A time sequence of the field of thunderstorm and gust echoes (Fig. 1) suggests that the gust propagated with a nearly constant velocity of 13 m s^{-1}. No thunderstorms were observed south of the one sketched in Fig. 1.

Figure 2 shows the Doppler velocity field of the gust at 2245 [all times CST (Central Standard Time)] when the beam elevation angle (EL) was fixed at 0.4° while the beam scanned azimuthally (AZ) from 327 to 43°. Note the abrupt change in radial velocities across the leading edge of the gust. The narrow SW–NE band of brightness (i.e., negative radial velocities) indicates a gust of air moving radially toward the radar; whereas the environmental wind on either side of the gust moves radially away (i.e., positive velocities tagged by less bright areas) from the radar with equal speed on both sides of the gust. This characteristic suggests that the gust is not the front of outflowing downdraft air (i.e., not a downdraft gravity current) but a solitary gust or wave. The small patch of brightness at a range of about 37 km and at AZ 356° is caused by the zero Doppler velocity echoes from a cluster of TV towers, one of which is the 444 m tall meteorological tower used for measurements reported in this paper.

Similar transitory phenomena are often observed in northern regions of Australia, although the source of the disturbance may not be a thunderstorm (Clarke *et al.*, 1981). Because the Australian phenomena are usually observed in the early morning hours, they have been given the name "morning glories." They are visually characterized by one or more cloud bands, which may be up to a few kilometers in width, extending laterally from horizon to horizon. Furthermore, the approaching wind gust can be heard from afar (Clarke, 1983). These cloud bands propagate with speeds of ~ 10 m s^{-1} in a direction perpendicular to the band. Aircraft and surface instruments have been used to examine the kinematic and thermodynamic structure of the atmosphere perturbed by these traveling bands and Clarke *et al.* (1981) suggest that these disturbances are produced by an internal undular bore which represents a stage in the evolution of solitary waves.

A similar phenomenon was photographed by E. Kessler (personal communication, 1970) in Central Oklahoma during early morning hours. Figure 3 shows a wave extending from horizon to horizon for

[1] Permanent affiliation: Academy of Meteorological Science, Beijing, Peoples Republic of China.

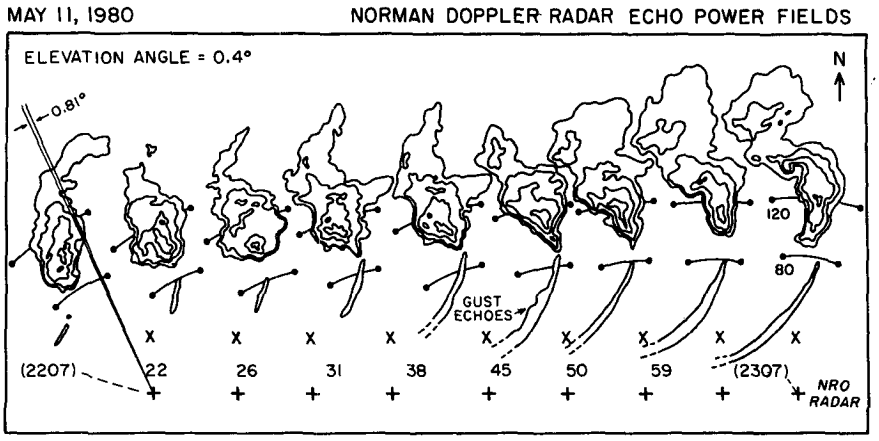

FIG. 1. Time sequence of echo power for a thunderstorm and a solitary gust for the period 2207 to 2307. Range arcs are 80 and 120 km; plus signs locate the Doppler radar, crosses the tower positions for each time. Reflectivity factor Z of the gust contour is ~0 dBZ with peak reflectivities of ~10 dBZ. Maximum reflectivity of the storm is ~55 dBZ. The 0.81° beamwidth of the radar is drawn to connect the Z data and radar position for the storm at 2207.

the dimension transverse to the direction of propagation whereas the length of the wave in the propagation direction is only a few kilometers. In the photo we see perhaps three waves; the radar reflectivity map also suggests more than one wave. These waves were behind the front of a gravity current which was detected by surface instruments. Furthermore, there were no significant wind perturbations on the surface that could be associated with waves. Thus, it seems that the waves shown in Fig. 3 are not part of an internal bore as suggested by the Australian observations but are, instead, atop the gravity current. In this regard they may be similar to those small amplitude waves observed on sea-breeze fronts (Simpson *et al.*, 1977) and might be Kelvin-Helmholtz waves. On the other hand, Maxworthy (1983) has identified, in a laboratory experiment, solitary waves being produced on top of a gravity current by a sudden

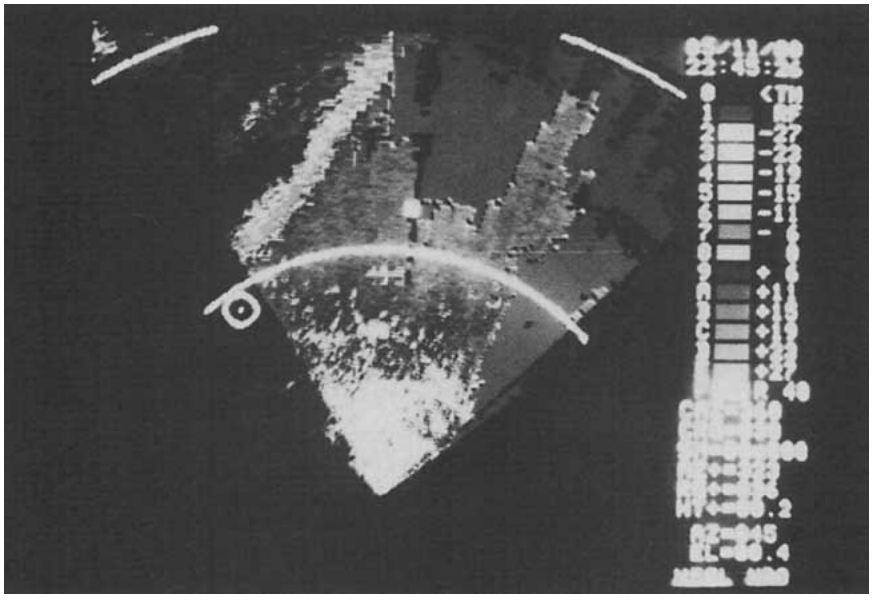

FIG. 2. Radial velocity field at elevation angle = 0.4°. The velocity scale (in m s^{-1}) is on the right of the photo. [A color presentation of the velocity field at an earlier time (2240) given by Rust and Doviak (1982) is more easily interpreted.] The uniform gray areas signify regions where data are deleted because overlaid multiple trip echoes made velocity estimates inaccurate. The bright clutter areas to 10 km ranges are ground target echoes. Range arcs are 40 km apart.

change in its flow rate. Furthermore, Haase and Smith (1984) report recent observations of wave clouds over Oklahoma seen from the surface, as well as from a satellite, but which appear to be part of an internal undular bore. In conclusion, there are insufficient data to make a definite identification of the type of waves shown in Fig. 3.

Observations by Christie and Muirhead (1982) underline the fact that Australian solitary-wave disturbances almost invariably occur in clear air and thus are usually undetectable by eye. The paucity of solitary wave reports in Oklahoma may also be a result of the lack of well-defined roll clouds. On the other hand, because longevity of these waves requires the temperature inversion usually associated with nocturnal air, observations could be rare due to the poor visibility at night and the lack of observers. Furthermore, Christie *et al.* (1978) have noted that the most significant meteorological observation associated with solitary waves is that surface temperature and humidity are not perturbed by their passage and that these waves appear to have no lasting influence on the surface wind. The capability of Doppler radar to survey vast areas of the lower atmosphere and to detect clear air perturbations above the surface can yield more data on the kinematic structure of these intriguing phenomena.

Solitary waves or gusts have been remotely observed with acoustic sensors (Christie *et al.*, 1981). Measurements with remote sensors can often provide an instantaneous picture of the evolving three-dimensional kinematic and reflectivity structure of these solitary disturbances and should complement measurements made with surface and airborne *in situ* sensors. The tall tower and Doppler radar observations reported here coupled with theoretical studies should thus help us to better understand atmospheric solitary waves.

In this paper, we compare *in situ* measurements made with the tall tower and surface instruments with those remotely measured by the Doppler radar. In Section 2 we describe briefly the tower and radar facilities; Section 3 gives data on the environment into which the gust propagated, and Section 4 gives data on the solitary gust. In Section 5 we provide arguments to convince the reader that the gust is a solitary wave generated by a thunderstorm. Although Doppler radar data were collected until 2318 when the gust had passed the tower, the data after 2245 were significantly contaminated by ground clutter, including echoes from several tall towers near the instrumented one. Therefore, only Doppler radar data at 2245 were combined and compared with tower data, as shown in Sections 3 and 4. The gust was then only 18 km from the tower, and because the gust appeared to have nearly steady intensity, the combination of radar and tower data and their comparison appears warranted. Finally, comparison of streamlines with equivalent potential temperature contours suggests this solitary gust may be a solitary wave.

2. The Doppler radar and tall tower

The National Severe Storms Laboratory's (NSSL's) 10 cm Doppler weather radar in Norman, Oklahoma, has a beamwidth of 0.8° and transmits pulses in alternating batches of two different pulse repetition frequencies (PRFs) allowing range-ambiguous targets that overlay into first trip targets to be flagged whenever they could cause significant error in the Doppler velocity field (Doviak *et al.*, 1978; Hennington, 1981). Areas of overlaid echoes are indicated by the uniformly grey areas in Fig. 2.

The 450 m tall KTVY-television tower, located 37 km north of the radars, is equipped for meteorological observations; Fig. 4 lists the parameters measured by this multilevel facility. Meteorological parameters were sampled every 10 s, digitized and recorded on magnetic tape for later data processing, quality control and conversions to meteorological units. On this day, the tower top pressure measurements were not available. Pressure at each level was inferred from the measured variations at the surface and a log-linear interpolation to each level assuming a 50 mb pressure

FIG. 3. Photo of a roll cloud that suggests the presence of a solitary wave. The arrow indicates the position of the clearly identified roll-type cloud. View is north from NSSL. The radar reflectivity fields on the right side show at least four thin line echoes that might be associated with four waves.

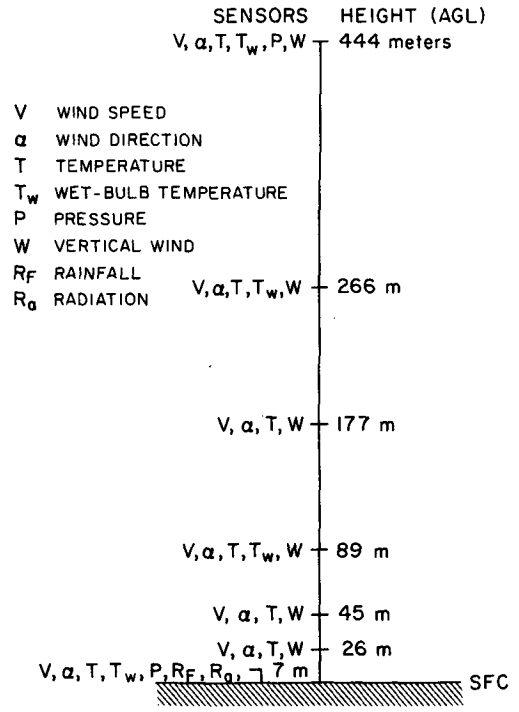

FIG. 4. Tower sensor configuration.

difference, between the surface and 444 m, which is the average observed over long periods of time during nondisturbed atmospheric conditions. We have also integrated the hydrostatic equation, using temperature data from the tower, to deduce pressure at the various levels, and found this pressure agreed to within a millibar of those values deduced by assuming the 50 mb difference. Thus, loss of pressure data at the tower top should not severely compromise our estimate of vapor pressure and mixing ratios.

3. The environmental wind and temperature profiles

The NSSL Doppler radar can detect echoes over large rain-free areas at the 0.4° elevation angle as shown in Fig. 2, and also at higher angles in front of the advancing gust allowing Doppler radar wind soundings to 2 km altitudes. To determine the vertical profiles of horizontal wind, radial velocities at a range of ~40 km and less to the north of the radar were averaged over 1 km range intervals along each beam position to reduce the statistical fluctuations in the estimate. These fluctuations are caused by turbulence as well as electronic noise in the radar's receiver, especially when echo intensity is not large compared to the noise power, as is the case here. Two averaged

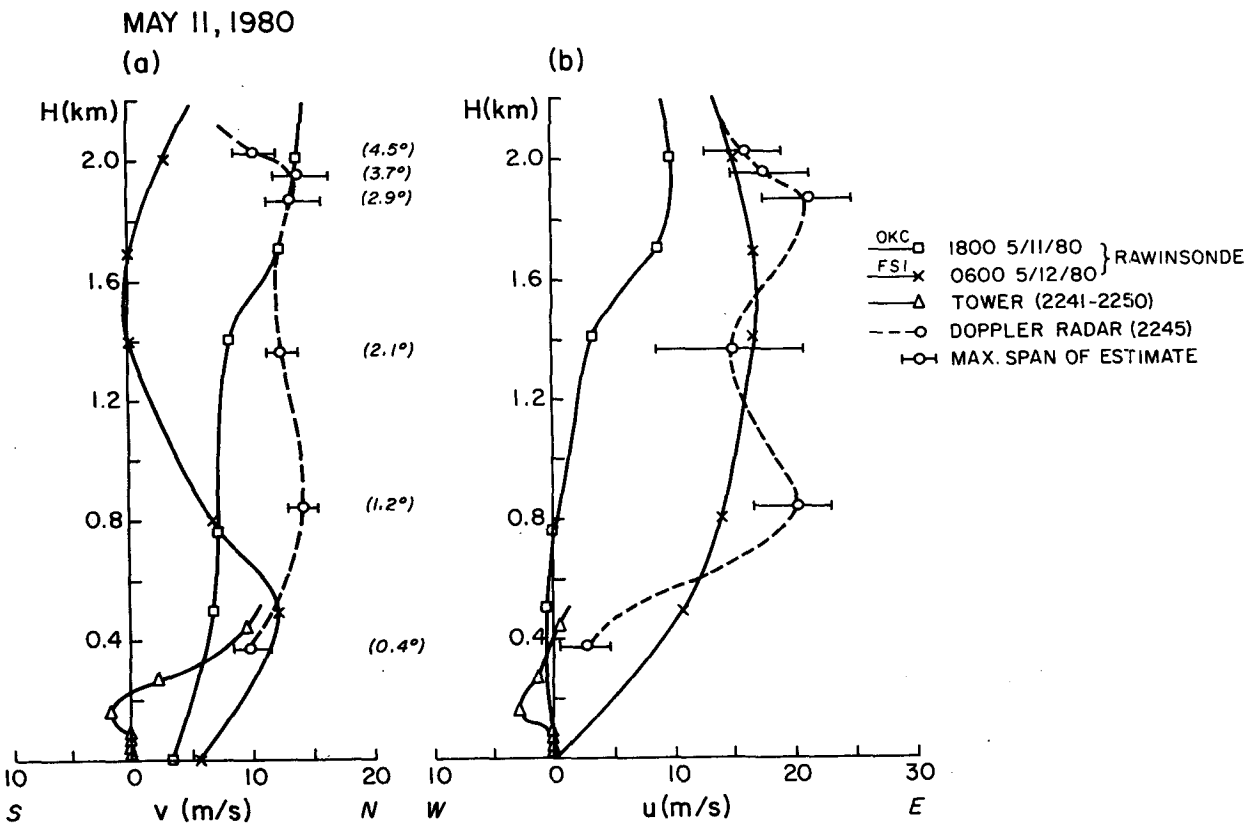

FIG. 5. Vertical profiles of the ambient wind observed by Doppler radar, tower and rawinsonde. The rawinsonde sites are ~20 km NW (OKC) and 120 km SW (FSI) of the Norman Doppler radar. The Doppler radar estimate of wind is an average over a 40° sector 40 km north of the radar. (a), (b) The north and east components of wind. (c), (d) The wind components parallel and perpendicular to the cross section shown in Fig. 7.

radial velocities separated by 25° of azimuth for each elevation angle were used to estimate the wind speed and direction under the assumption that the wind was uniform over the region southeast of the advancing gust. Data from ten contiguous (i.e., 1 degree of azimuthal spacing) pairs were averaged to obtain a mean value of the environment wind speed and direction. The north–south and east–west components of the mean wind profile are plotted in Figs. 5a, b where the horizontal bars show the range of values for the ten wind estimates made at each of the indicated heights. Data from the several elevation angles marked on the figure were used to construct this wind profile.

Rawinsonde wind profiles 5 h before and 7 h after the events are also plotted in the figure to show how much the wind changed during the 12 h interval. The wind speed and direction below 500 m are obtained by averaging over a 10 min interval, the tower wind data at seven levels (7, 26, 45, 89, 177, 266 and 444 m).

The tower wind profile connects well with that deduced by radar, but because blockage of the beam's radiation and terrain reflection prevents accurate radar observations at low elevations, only the wind at the tower top can be meaningfully compared with radar data. Comparing the wind data from tower and radar at the 444 m level, we do see significant differences. However, the radar estimates are averages over a large volume of space, whereas the time averages of tower data correspond to an average along a line. Furthermore, even though the beam axis is pointed above the horizon by one-half the beamwidth, reflections from the terrain surrounding the radar and blockage by nearby buildings and trees, whose elevation angle is equal to or less than 0.2°, may still distort the radiation pattern of the antenna (Beamer, 1970). Blockage of the lower portion of the beam

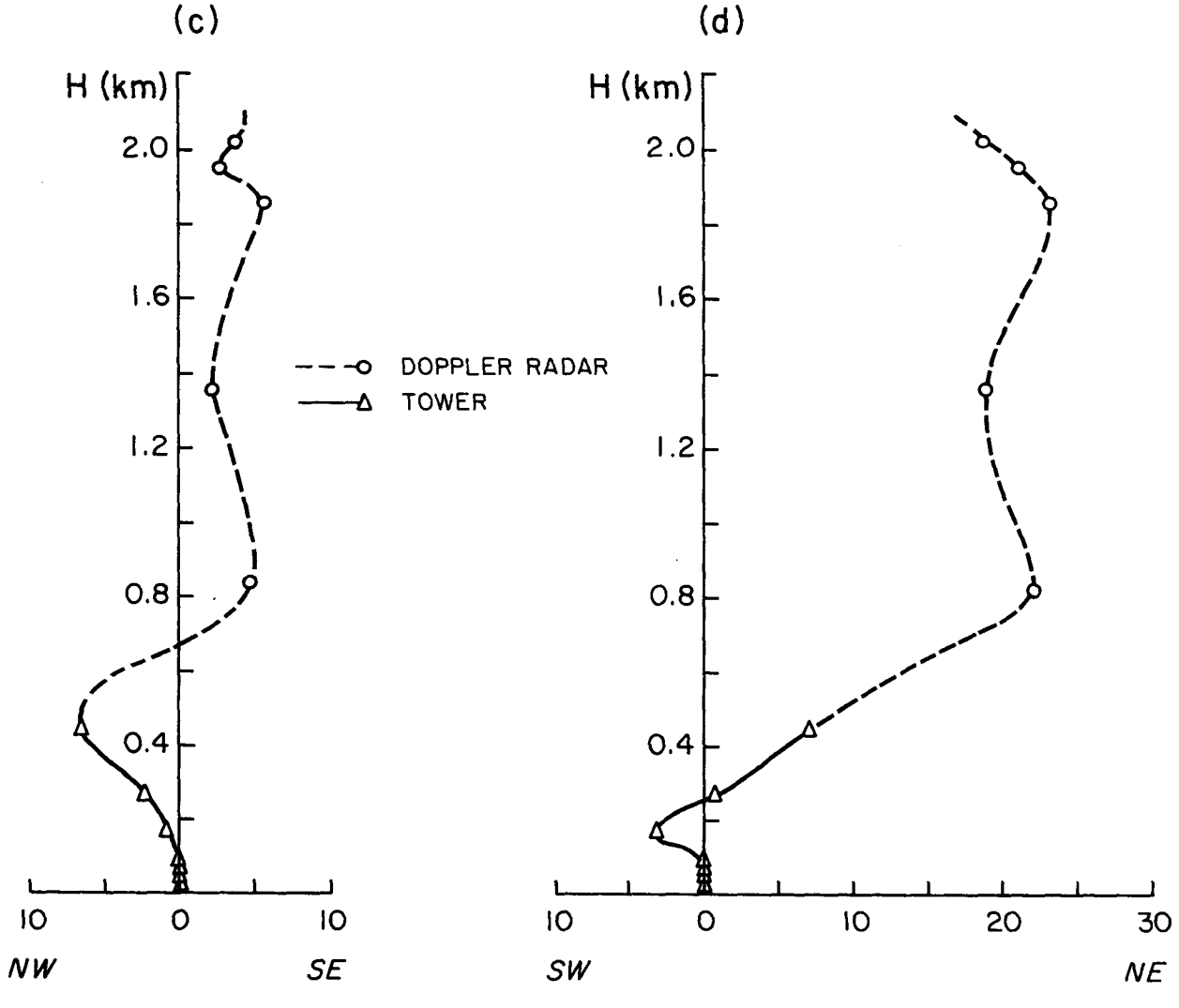

FIG. 5. (*Continued*)

then causes velocities in the beam's upper portion to have relatively more weight in the Doppler velocity estimates. Thus, the difference in tower and radar wind measurements may be explained, although detailed examination of beam shape and reflectivity distribution would be required to prove this hypothesis. Although both estimates may be accurate, the radar data should be more representative of the mean ambient wind when the elevation angle is more than a half beamwidth above the horizon, provided that the reflectivity distribution is uniform within the beam. Furthermore, because the radar also measures wind above the tower top, both measurements are complementary.

Figures 5c, d are plots of the vertical profiles for wind components in directions parallel and perpendicular to the NW–SE cross section (see Fig. 7). The radar data have been smoothly connected to tower data at the 444 m height. These profiles are the ambient wind components parallel and perpendicular to the gust front, and we see that the magnitude of the vertical shear is stronger than 4×10^{-2} s^{-1} in the height region 200–800 m, and the wind is relatively uniform above 800 m. Furthermore, the wind and shear are strongest for the wind component in a direction along the gust front. This has an important bearing on the permanency and speed of solitary waves, as discussed later in Section 5c.

Figure 6 shows the temperature profile measured by the tower for the 10 min periods before and after the gust, as well as the profiles obtained from rawinsonde 5 h before (1800) and 7 h after (0600) the passage of the gust. The Oklahoma City rawinsonde site (OKC) is located ~15 km south of the tower and the Fort Sill site (FSI) is ~100 km to the southwest.

The dashed line above 444 m is a subjective estimate of the temperature profile just before the gust passage and connects the tower data averaged in the 10 min interval before the gust. The lower solid curve is the temperature profile for a 10 min period after gust passage. The gradient Richardson number R_g is computed using the inferred temperature profile and windshear from Figs. 5c, d. The tower data before and after the passage of the gust shows that it modified the boundary layer air. Slight cooling at the 444 m level and warming at lower levels indicates that some mixing took place, although there is little of the net change of air mass that would occur if the gust were caused by a gravity current of thunderstorm outflow air.

4. Solitary gust observations

The gust was first detected at 2207 CST (Fig. 1) when it was still at a range of ~70 km from the radar. Buildings and trees near the radar that blocked radiation at elevation angles below 0.2°, and the earth's curvature prevented earlier observation of the gust whose radial velocity perturbation was strongest below 1 km (see Section 4b).

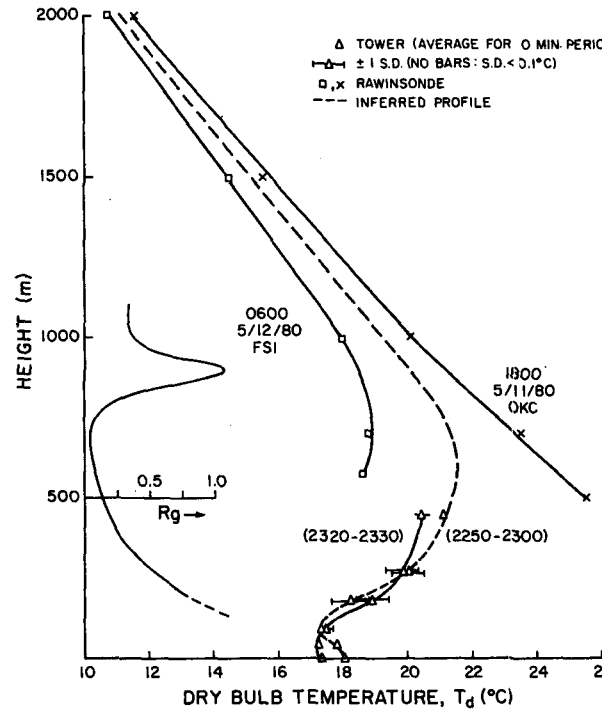

FIG. 6. Vertical profiles of temperature measured by rawinsonde and tower within the first 2 km, and the gradient Richardson number R_g profile.

The reflectivity field of the storm associated with the gust is depicted at different times in Fig. 1, showing the storm to be relatively steady with reflectivity factors larger than 45 dBZ as it tracked toward 58° at a speed of 23 m s^{-1}. Although the storm produced hail and tornadoes, substantial damage was not reported. The environmental wind speed deduced from Doppler radar for the altitudes 1–2 km AGL is 27.5 m s^{-1} toward 54° (Fig. 5).

Figure 7 shows isochrones for the gust as determined by Doppler radar observations of the leading edge of zero Doppler velocity. [This figure suggests the gust had a speed and direction (13 m s^{-1}, 312°) different from that of the storm.] The cloud-shaped structure sketched in Fig. 7 indicates the width of the gust's reflectivity field. Superimposed on this plot are locations of surface sites where the time of gust passage was determined as the time at which surface wind had a sudden rise. Time of arrival of the gust is indicated at each site, and good agreement is found between data from the two independent measurements. The peak surface wind speed (m s^{-1}) behind the leading edge of the gust is tabulated to the right of the gust arrival time at the surface site. Surface data suggests that the gust weakened as it propagated southeastward, and at the surface site less than 10 km from the radar, and at the radar itself, no gust was evident. However, the gust may still have been

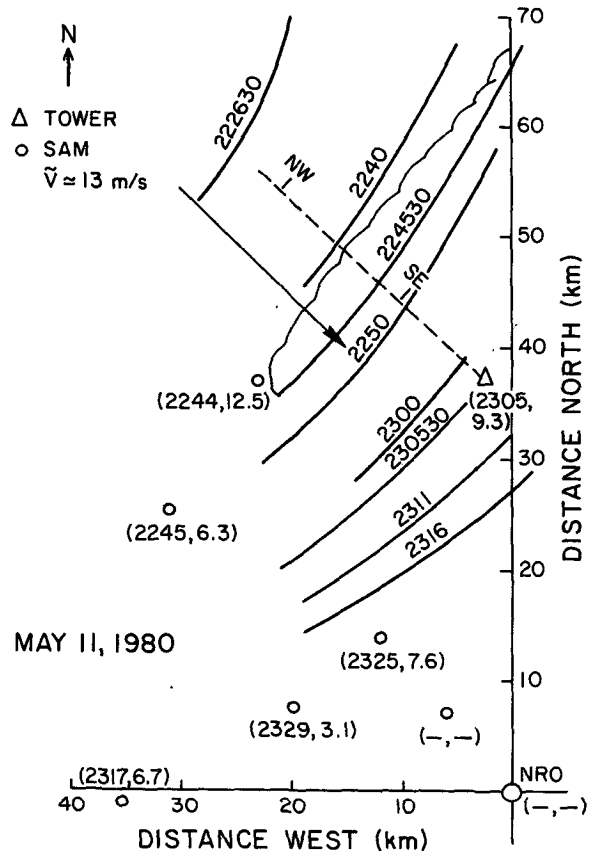

FIG. 7. Isochrones of gust position and location of tall tower, sites of the automated meteorological instruments (SAM) and radar. The arrow indicates the approximate direction of gust motion and the dashed line is the location of the cross section of the gust observed at the tower but translated in time to the 2245 position where radar data are available for comparison. The time of arrival of the gust at each surface site is indicated in parentheses next to the station where peak gust speed (m s^{-1}) is also listed.

present above the surface because it sometimes leaves no discernable marks on surface temperature and wind traces (Christie *et al.*, 1978).

Figure 7 also shows the location of the tall tower (Range = 36.98 km and AZ = 356.36°), NSSL's Doppler radar (NRO) at Norman, Oklahoma, and the NW to SE cross section (dashed line) along which the 2245 CST Doppler data field was compared and combined with time series data from the tower.

At the time of radar data collection, interest was focused on the storms to the north and not on the gust, so the sector limits of azimuthal scan were not set to display fully the length of the gust. Thus, the line length variations in Fig. 7 are due principally to lack of observational data.

a. Vertical velocities

In Fig. 8 we have plotted the vertical velocity versus time (2300–2350) for the 177, 266, and 444 m tower levels. It is apparent that there is a coherent wavelike perturbation that exists during the period 2305–2320. In the 10 min time interval before 2305, the vertical wind at the 444 and 266 m levels averaged 0.72 m s^{-1} with standard deviation S.D. = 0.6 m s^{-1} and −0.1 m s^{-1} with S.D. = 0.2 m s^{-1} respectively. During this same period, the southerly horizontal wind at the same two levels is quite steady at ~10 m s^{-1} (S.D. = 0.7 m s^{-1}) and 4 m s^{-1} (S.D. = 1.2 m s^{-1}) respectively. There was no substantial change in wind characteristics for several 10 min periods before the arrival of the solitary gust, except for fluctuations of the average vertical velocity about zero at 444 m.

The rms deviation in vertical velocity is ~0.5 m s^{-1} around the dashed curve (Fig. 8), which is a subjective fit of the coherent part of the solitary gust. Note the cusplike peaks seen at all the levels and the stronger downward motion in the wave portion of this trace. At 2321 there is a sudden onset of turbulence in which the vertical wind has a very short time coherence with no apparent spatial coherence between the tower levels and is unlike the temporal and spatial coherence of the solitary gust or wave. This turbulence has peak vertical velocities (6.6 m s^{-1}) that exceed those observed in the wave, and shears are correspondingly stronger. However, it also appears that the 10 s sampling interval is too coarse; therefore, perhaps even higher vertical velocities may have been missed. The turbulence apparently ends at about

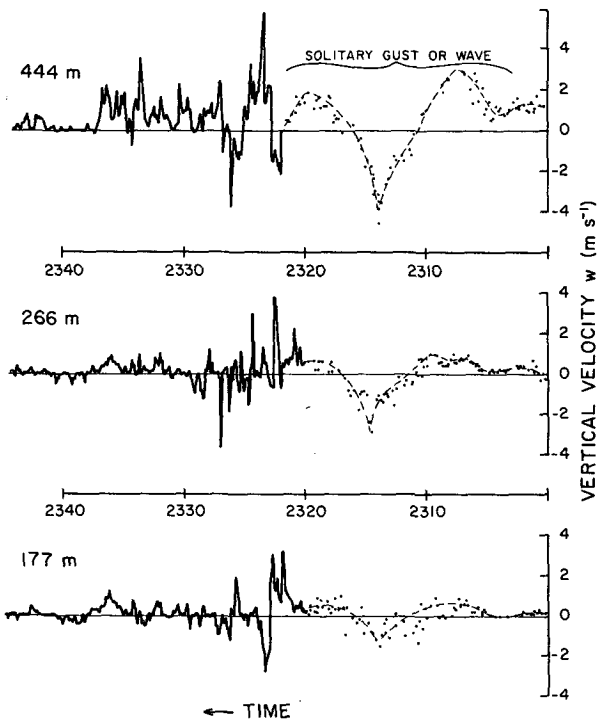

FIG. 8. Vertical velocities at the three upper tower levels for the time period 2300–2345. Each 10 s sample value is indicated by a dot. The dashed line graphs the subjectively interpreted vertical velocity of the wavelike portion of the solitary gust. The solid line connects each 10 s sample in the turbulent region.

2348. We suggest that this turbulence was caused by wave-induced local increases of wind shear (see Section 5 for further discussion).

b. Solitary gust streamlines

In Fig. 9 we have plotted 2-minute samples of the horizontal and vertical winds projected onto the NW–SE cross section depictetd in Fig. 7. The winds perpendicular to this cross section showed significantly less variability. The tower-inferred winds are the lightly traced arrows, which indicate the horizontal and vertical speeds if the indicated speed scale is used. The streamlines are subjectively drawn to be tangent to the plotted wind vectors after they are adjusted in proportion to the ratio of horizontal to vertical distance scales. Because the gust translated at the nearly uniform speed of 13 m s^{-1}, we have deduced the horizontal scale indicated on this figure.

Detailed wind data exists only below 444 m, so the dashed lines in Fig. 9 are only guesses as to how the streamlines connect. The diminution of wind speed at the upper levels of the tower suggests a null and reversal of horizontal wind 100–200 above the tower. Furthermore, we assume that the uniform wind, observed with the Doppler radar on an azimuthal scan at the next elevation angle (1.2°), indicates that streamlines above those sketched in Fig. 9 are essentially equispaced along the vertical. A more accurate tracing of the upper streamlines would have been possible if Doppler data were acquired at an 0.8° elevation angle. Although there was no evidence of a velocity perturbation at EL = 1.2°, Doppler data at higher elevation angles (i.e., 2.0°) showed some hint of much weaker (i.e., ~4 m s^{-1}) wind perturbations aligned along, and about 2 km above, the gust. At this altitude there appeared to be a lowering of Doppler velocities a few kilometers in advance of and behind the gust, whereas the winds directly above had speeds close to that of the quiescent atmosphere. These observations suggest that the disturbance extended to altitudes of at least 2 km and that streamlines above 1 km are not equispaced along the vertical, but are progressively stretched horizontally with further increases in height. Unfortunately, echoes were weak, causing poor data quality, and association of these weak perturbations with the gust remains uncertain.

c. Temperature, water vapor and total pressure characteristics

The cross section of dry-bulb temperature T_d (°C) and water vapor pressure p_w (mb) is plotted in Fig. 10, showing that the core of this solitary gust is cool and dry with centers located about 300–500 m AGL. A temperature decrease of 5°C is noted as the gust passes the tower, but the temperature quickly recovers nearly to its pre-gust value. Likewise, p_w has a 7 mb depression at an altitude of 444 m.

The lower trace shows that surface pressure increased to a peak 1.3 mb above its quiescent value of ~964.7 mb. In this regard, it should be noted that pressure peaks less than 1.1 mb observed with an

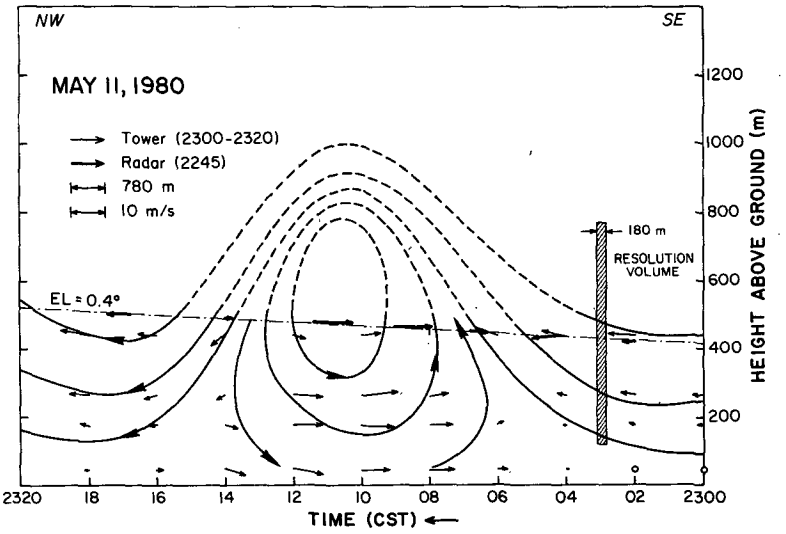

FIG. 9. Samples of winds (lightly traced arrows) measured at tower at four levels in the NW–SE cross section (Fig. 7) of the gust for the time period 2300–2320. The velocity scale is listed in the upper left corner and applies to both the horizontal and vertical speeds. Bold arrows are Doppler radar estimates of wind at 2245 projected onto this cross section. The dashed streamlines are subjectively estimated in the data void region between 500 and 1000 m.

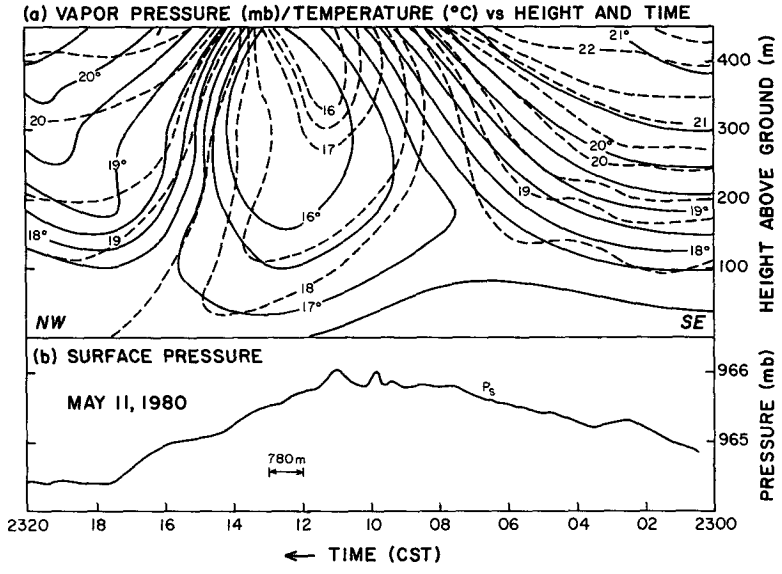

FIG. 10. (a) NW–SE cross section of the gust's temperature and water vapor pressure as measured by the tall tower. Solid lines are temperature (°C) in steps of 0.5°, and dashed lines are vapor pressure (mb) in steps of 0.5 mb. (b) Surface pressure (mb) at the tower position.

infrasound array in Australia have been associated with solitary waves (Christie *et al.*, 1978). The whole event lasted approximately 17 min which, using a propagation speed of 13 m s^{-1}, corresponds to a spatial distance of ~13 km. After the pressure hump of the gust passed, the pressure increased slowly and at about 2330 it attained its pre-gust value with only small (i.e., $\Delta p \leq +0.2$ mb) pressure perturbations.

5. Discussion

More than one interpretation may explain the observations. For example, the gust could be a cylinder of cool thunderstorm outflow air that has been severed from its thunderstorm source and, as it slips unaltered southeastward at speeds of about 13 m s^{-1}, boundary layer air is lifted and cooled. Thus, a negatively buoyant cylindrical vortex could be translating along the surface.

The long lifetime of this solitary gust must indicate weak dissipative effects or some source of energy; the statically stable boundary layer without surface-based convection in the evening may have allowed the gust a long life. It would be important to establish whether only nighttime thunderstorms produce solitary gusts and whether they are stronger and more persistent than those which might be launched by daytime storms.

a. Observations compared with laboratory experiments

The laboratory experiments of Maxworthy (1980) have relevance to the interpretation of our data. He observed the evolution of the structure of a fluid intruding into a narrow region of strong vertical density gradient (pycnocline) separating two homogeneous fluids. His observations can be related to the intrusion of cold and dense thunderstorm downdrafts flowing along a surface-based inversion, if one can assume that the effect of small density changes on the inertia of the fluid is negligible (i.e., the Boussinesq approximation). Then the space below the plane of symmetry of the density gradient may be regarded as dynamically similar to the space above, and for antisymmetric motions, a rigid boundary could be placed at the interface (Benjamin, 1967). Such antisymmetric waves were observed in laboratory experiments, and motions above a rigid boundary should be approximately the same as observed by Maxworthy, even though his experiment did not use a rigid interface. Thus, his observations of fluid motions in the upper half space could represent motions of air above the earth's surface.

The intruding fluid, marked by dye and having a density equal to that at the interface, is made to penetrate the pycnocline by the removal of a barrier that separates the intrusive fluid from the one containing the pycnocline. As the intrusive gravity current progressed along the pycnocline, and diminished in amplitude, bulges of forming waves began to emerge. The first was at the current front and others behind, each successive wave having an amplitude less than the one ahead. A compact blob of intrusive fluid was seen to be circulating inside each wave of large amplitude. Because of internal mixing and energy

dissipation, the wave amplitude decreased, and caused the intrusive fluid to slowly leak from the rear of the waves until eventually no closed circulations were observed. At this point, the waves continued to propagate at nearly constant amplitude and shape (i.e., they were solitary waves of permanent form), and traveling at constant speed they eventually left the gravity current behind completely.

Thus, there is the possibility that the outflow of the observed thunderstorm (Fig. 1) launched a solitary wave which propagated at the speed of 13 m s^{-1} and, that the lifting of boundary layer air by the wave is responsible for the observed intense local cooling at the upper levels of the tower.

On the other hand, environmental air may also be lifted by the intrusion of a horizontally oriented elliptical cylinder of cool and dense outflow air. The fact that the cold pocket (Fig. 10) is behind the peak of streamlines (Fig. 9) supports this idea. Furthermore, if the gust is a cylindrical pool of cool dense air slipping along the ground and penetrating warm and less dense ambient flow, then lines of constant potential temperature in the denser air would begin and end on the surface, although the ambient air would have isentropes asymptotically approaching the surface. But if the observed gust is a solitary wave of permanent form without thunderstorm outflow, the lines of constant potential temperature (isentropes) would have a humped shape, as theory shows, and they could not intersect the surface. Because the air is so moist, there is, as stated earlier, the potential for precipitation to form and fall out of a parcel of air. However, contours of equivalent potential temperature θ_e, which is a conserved property even with change of moisture phase, delineate air parcel trajectories if the wave is steady, as Doppler radar observations suggest. Thus, in Fig. 11a, we have plotted the contours of θ_e along the NW to SE cross section. Although we notice some isentropes intersecting the surface, which suggests that there is cold air blocking the ambient flow, the isentropic pattern is more suggestive of a wavelike perturbation.

Furthermore, whereas the speed of the solitary wave is determined by the characteristics of the invaded media, and to a lesser extent by the wave's amplitude (Benjamin, 1967), the speed of the gravity current is proportional to the square root of the depth of current behind the head and the difference in density of the current and the ambient air (Britter and Simpson, 1981). For a finite volume of intrusive fluid, as we must have for thunderstorm outflows, the depth, and hence the gravity current speed, must continuously decrease; whereas, a solitary wave of permanent form has a constant speed of propagation. Because a cylindrical pool of denser outflow air would be continually acted on by the force of gravity, the outflow air would flatten and widen progressively with time. This process should cause a noticeable change in the ambient flow pattern because the front and back edges of the solitary pool should move in opposite directions at the approximate speed $v \approx (gh\Delta\theta/\theta)^{1/2} \sim 2.6$ m s^{-1}, where $h \approx 200$ m is the depth of the cold air and $\Delta\theta \sim 1$ K is the potential temperature difference between the outflow and ambient air. But the Doppler radar observations show no measurable change in the solitary gust for at least a 40 min period although the leading and trailing edges of the cylindrical pool should have separated by more than 12 km. Thus, we are led to conclude that although storm outflow may be present, it is

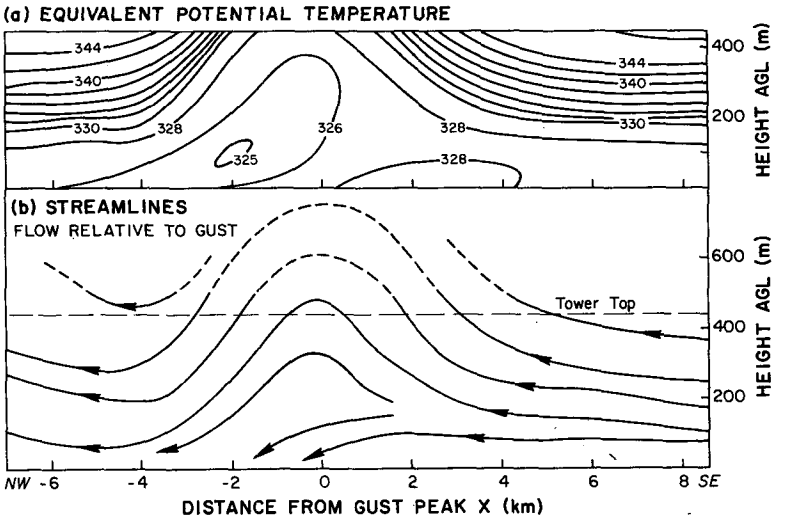

FIG. 11. (a) Equivalent potential temperature (K) in the NW–SE cross section of the solitary gust. Contours are stepped in 2°C intervals. (b) Streamlines in a coordinate system moving at the gust velocity.

trapped in a wave that is also lifting the ambient air causing the observed large drop in temperatures. The position of the cold air pocket relative to the peak of the streamline trajectory is evidence of the trapping.

Because parcel trajectories inferred from Fig. 11a are those relative to the gust, we cannot compare it to streamlines of Fig. 9, which are relative to the ground. So we have, in Fig. 11b, plotted the observed streamlines in the coordinate frame moving along with the gust. The comparison of the two figures shows a close similarity between observed streamlines and contours of θ_e, also suggesting a nearly steady flow in accord with radar observations. It is to be noted that the relative flow is through the disturbance at all levels and that there is no evidence of advected flow.

Maxworthy (1980) also observed in laboratory experiments that a large amplitude solitary wave, containing circulating fluid from the gravity current which produced the wave, achieved a critical Richardson number at the rear of the wave where mixing took place. Taking note of the increased level of turbulence behind the atmospheric wave (Fig. 8) and the low values of Richardson numbers (Fig. 6) in the ambient air, it is likely that the turbulence is caused by the wave, which may have reduced the Richardson number below its critical value for the onset of breaking Kelvin–Helmholtz waves and turbulence at the lower heights. Furthermore, the 2320–2330 temperature profile (Fig. 6) suggests that turbulent mixing has increased the lapse rate of sensible temperature from its value at 2250–2300 prior to the passage of the gust. The striking similarity between the fluid flow in the laboratory and the wind field in the atmosphere suggests that we indeed have observed the same type of phenomena in nature as that simulated in the laboratory.

b. Solitary wave characteristics

Christie *et al.* (1978) presented the first convincing evidence and arguments that solitary waves of permanent form can and do, in fact, exist in the atmosphere on surface-based inversions. In order to determine whether the observed nocturnal solitary gust fits the characteristics of a solitary wave, we summarize the latter's features:

1) A solitary wave is a single-crested disturbance. But one or more of these can evolve from an arbitrary initial disturbance which itself could be of relatively large scale with weak shear. In the context of a thunderstorm, the cold-air outflow may cause such an initial disturbance of large scale, out of which one or more waves can emerge while the disturbance travels at the long-wave phase speed (Christie and Muirhead, 1983a,b).

2) Solitary waves grow in amplitude as their width decreases, thereby increasing shear, and their speed exceeds the long-wave phase speed by an amount proportional to wave amplitude. Thus, solitary waves have supercritical speeds and can propagate out ahead of the thunderstorm outflow gust front and be far from the thunderstorm that generated it. Yet, these waves can harbor shear that could be hazardous to safe flight. Christie and Muirhead (1982) show, through numerical simulations, how disturbances of long wavelength evolve into short solitary ones. Supercritical waves of this type are usually observed to propagate with speeds between 6 and 16 m s^{-1}. Assuming that the ambient air velocity in the NW–SE direction is zero (Fig. 5c), the solitary gust reported herein had an observed speed of 13 m s^{-1}. However, evidence (Fig. 7) suggests that the phase speed is decreasing with time (from 15 m s^{-1} at 2226 to approximately 10 m s^{-1} at 2316).

3) The number of waves that evolve depends on the scale size of the initial disturbance—the larger it is, the larger the number of waves that can be generated (Whitham, 1974, p. 595). In the case reported here, there is evidence of only one strong wave followed by at least one weaker wave, as will be shown in Section 6.

4) Long waves of small amplitude experience little dispersion and accompanying change in shape, whereas short waves of small amplitude disperse quickly. However, long waves of large amplitude break, while large amplitude solitary waves of permanent form require wavelengths to be short. Thus, the tendency of waves to break because of the nonlinearities at large amplitude is balanced by the dispersion which tends to smooth the shorter wave. However, this inverse relation between wave amplitude and half amplitude width required for solitary waves ceases when the wave width decreases to approximately two to three times the pycnocline thickness Δh, at which point recirculation in the wave increases, causing the width to increase (Tung *et al.*, 1982). Furthermore, the numerical solutions of Tung *et al.* (1982) for the case of strongly nonlinear waves (i.e., wave amplitude $\geq 0.25\ \Delta h$) show that circulation begins in the solitary wave when wave amplitude to pycnocline thickness is about 0.45.

Although the pattern in Fig. 11b does not show any closed streamlines, it appears to be on the verge of a closed circulation. The presence of so few closed contours in Fig. 11a, and the absence of them in Fig. 11b, suggests that recirculation of air, if present, is weak. Furthermore, assuming a 500 m pycnocline half thickness from Fig. 6, and because the observed wave amplitude (Fig. 11b) is no more than ~400 m, the application of the Tung *et al.* (1982) results, described above, also leads one to conclude that the wave is on the verge of having an internal circulation. If some recirculation were present, we would then expect the half amplitude width to be about two to

three times larger than the pycnocline's Δh. For the estimated 1000 m pycnocline thickness, the minimum half amplitude width would then be ~2.5 km, whereas the width of the observed wave is ~4 km. Although stronger circulations can increase the width, there is little observational evidence (Fig. 11b) of any circulation. The larger observed width, and an amplitude less than that required for recirculation, is consistent with conditions necessary for waves to have a permanent form. That is, the weaker amplitude wave must be accompanied by a larger width in order to maintain the balance between the effects of dispersion, which tend to spread and smooth the wave, and those of increased nonlinearity at larger amplitudes, which tend to sharpen the wave. Thus, sharpening, if unchecked by dispersion, could lead to wave breaking.

Radar at 2245 (see Fig. 2) shows the width to have an average value of ~4.5 km between Doppler velocity reversals. The radar beam is centered then at an altitude of about 500 m. When the gust, translating at the speed of 13 m s^{-1}, reaches the tower 25 minutes later, the wavelength between speed reversals for flow in a direction toward the radar is ~3.1 km at the 444 m tower level and 5.5 km at the 266 m level. The reflectivity fields (not shown here) suggest that the reflectivity weighted Doppler velocity would be more appropriately located at lower altitudes than, as in Fig. 9, at beam center, which assumes reflectivity to be uniform throughout the radar's resolution volume. Thus, the 0.4° Doppler velocity data plotted in Fig. 9 may need to be shifted to slightly lower altitudes, which, incidentally, would bring the Doppler-observed velocities in closer agreement with those observed by the tower. Furthermore, the 4.5 km width observed earlier by radar would then be in better agreement with the tower-measured widths between the 444 and 266 m levels. Thus, evidence points to the fact that there may be no significant change in wave characteristics between 2245 and 2310. This is further substantiated by examining the amplitude of the Doppler velocity in the gust at earlier (i.e., 2226) times not shown here, which again supports the observation that the disturbance is relatively constant in amplitude as well as width for at least a 40 min period. Therefore, the dispersive forces, which tend to weaken and spread the wave, may be balanced by the effects of nonlinearity, which tend to sharpen it.

c. *Observations compared with numerical results*

Although most of the solitary wave characteristics listed in Section 4 fit the observations reported herein, it behooves us to make quantitative comparisons of the observed solitary wave streamlines and wind fields with those obtained from the numerical solutions of Christie and Muirhead (1982). They have calculated streamline patterns and wind fields based on a semi-empirical analytic solution which reduces, at low amplitudes, to the second-order solution derived by Grimshaw (1981). Christie and Muirhead consider an inversion of 500 m depth in which θ changes 10°; whereas, the inversion observed here is also ~500 meters deep and has a θ change of about 8.5°.

Although Christie and Muirhead ignore shear, observations here show that except for the first few hundred meters of the ambient atmosphere, which exhibits little or no shear, the wind veers with height and shear approaches values of 8×10^{-2} s^{-1} at 600 m altitudes. However, as can be seen from Figs. 5c, d, most shear occurs for the wind component having direction parallel to the gust front. Because of the two-dimensionality of the gust, we should not expect shear of this component to significantly modify the dynamical structure of the wave. Although the Richardson number of pertinence to the generation of Kelvin–Helmholtz waves and turbulence requires the use of vector wind shear, we assume it is the Richardson number associated with shear of the wind component perpendicular to the front that is of crucial importance in determining the alterations of the dynamical structure of the solitary wave. As we can see from the data, this Richardson number is larger than two. Tung *et al.* (1981) have examined the influence of shear on the shape and speed of solitary waves for R_g as small as two. They conclude the structure of the solitary wave of the lowest mode number (i.e., one for which there is no reversal in the vertical displacement of streamlines and the one most likely observed here) has no change in shape but has a slightly faster speed than solitary waves propagating in shearless environments. Therefore, shear should not compromise the comparison of our data with the numerical results of Christie and Muirhead (1982).

Figure 12a reproduces the streamline pattern calculated by Christie and Muirhead (1982) for a solitary wave that has an intensity slightly below the minimum amplitude required for recirculating flow. Also plotted in this figure is a streamline taken from Fig. 11b which shows remarkably close agreement in shape, amplitude and width. Using the calculated streamline pattern plotted in this figure, we have numerically evaluated the horizontal and vertical wind as a function of height z at the wave peak (vertical section A–A) and at x = 1560 m (vertical section B–B) either side of the peak. The model results are plotted in Figs. 12b, c showing that the horizontal and vertical winds relative to the gust increase with z at a rate close to that observed. Because we did not have absolute values of the streamfunction, we needed to find a scale factor to apply to the model wind. The slope of the model curves plotted in Figs. 12b, c are proportional to this scale factor. Thus, not only do the streamlines agree in shape, but also in density.

The above comparison and close agreement be-

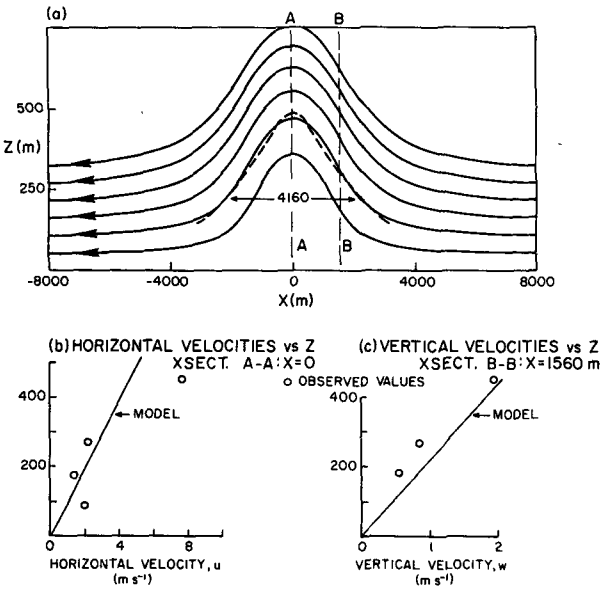

FIG. 12. (a) Comparison of solitary wave streamlines for a model (solid lines) with observed values (dashed line). (b) and (c) Comparison of solitary wave velocities for a model with those observed. The horizontal velocities in (b) are along the vertical line A–A on Fig. 12a and the vertical velocities in (c) are along the vertical line B–B.

tween numerical results and observed data also suggests that the observed solitary gust is a solitary wave that may contain little if any recirculating thunderstorm outflow air.

6. Concluding remarks

Although the solitary wave was far from the storm that apparently generated it, it still had significant horizontal and vertical shears (e.g., 7×10^{-3} s^{-1} and 6×10^{-2} s^{-1}) of the horizontal wind. To give a perspective on the significance of such shears on aircraft performance, note that a decrease in headwind along an imagined 3° glide slope through the solitary wave is larger (19 m s^{-1}) than the one that caused a 50 m drop in altitude of a 747 aircraft on its approach into Melbourne, Australia (17.5 m s^{-1}; Woodfield, 1983). Furthermore, turbulence behind the wave possessed even stronger horizontal shears with wind changes as large as 6 m s^{-1} over 130 m distances, or a shear value near 5×10^{-2} s^{-1}. An aircraft landing at a speed of 140 knots (72 m s^{-1}) could experience a 12 k (6.2 m s^{-1}) headwind decrease in ~2 s. Gossard (1983) and Bedard *et al.* (1979) have already recognized the possible hazards to aircraft posed by gravity waves. More recently, Christie and Muirhead (1983a,b) have shown how an initially smooth long wave with relatively benign shear can evolve under the influence of amplitude and frequency dispersion into an amplitude-ordered family of solitary waves of large amplitude and short half-amplitude widths, in which shear is markedly increased. Their work suggests that the intense, transient shear zones generated with these waves constitute a serious hazard to the safety of flight at low altitudes. Even though there was no measurable rainfall in the gust, the Doppler weather radar was able to detect and make reasonably accurate measure of its velocity and turbulence fields.

Of significance to our observations is the influence that the atmospheric pycnocline intensity has on the generation and propagation of solitary waves. Gravity currents invading homogeneous incompressible fluids apparently do not generate solitary waves; whereas, gravity currents on pycnoclines quite easily generate them (Maxworthy, 1980). Although the atmosphere has a permanent pycnocline with maximum gradient at the surface, the temperature gradient must have a lapse rate $-dT/dh$ less than the adiabatic one, in order to sufficiently stabilize the atmosphere so that solitary waves can be generated. Furthermore, stability will suppress turbulence which would dissipate the waves.

Enforcing the latter idea is the fact that, on this day, a larger thunderstorm passed two hours earlier along the same track as the one depicted in Fig. 1. Although it did not produce a solitary wave, it did generate a current of cool air, which passed the tower at approximately 2145 (Fig. 13), dropping the surface temperature 1°C in ~7 min; whereas, for the one-and-one-half-hour period prior to its passage, and one hour after, there was no significant change in surface temperature. Although there were gusty winds associated with the current's passage, there was no evidence of a wavelike perturbation, as seen in Figs. 2 and 8, and the temperature change was small at the upper levels of the tower. Thus, we conclude that the atmosphere was not sufficiently stable to allow the development of solitary waves, even though the strength of the downdraft gravity current may have been at least as strong as the one which produced the solitary wave reported here. A likely scenario is that the earlier thunderstorm laid down a layer of cool air that established a sufficiently strong surface-based inversion so that the outflow of the subsequent storm (Fig. 1) could generate solitary waves.

This scenario may also explain the absence of solitary-wave wind perturbations at the two surface sites near the radar (Fig. 7). The leading edge of the gravity current, propagating at the estimated speed of 2.6 m s^{-1} passed the tower 100 min before the solitary wave which propagates at the faster speed of 10 m s^{-1}; the gravity current would have been overtaken by the wave at a line about 20 km southeast of the tower. At that location, the wave no longer has the gravity current generated surface-based inversion on which to propagate further, and it likely dissipates before reaching the two surface sites. An analogous result can be seen in a laboratory simulation in which solitary waves are generated atop a gravity current of

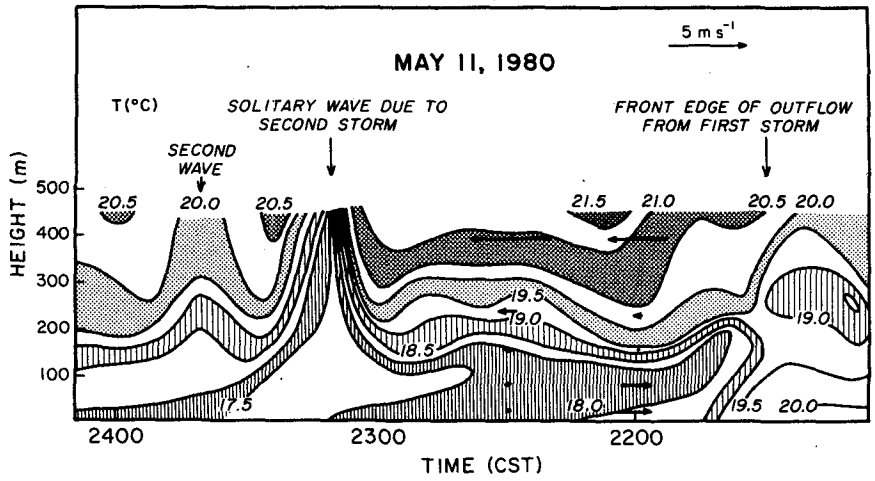

FIG. 13. Time–height cross section of temperature showing evidence of a gravity current from a thunderstorm and solitary waves produced by a second thunderstorm. Arrows are the wind components in the NW–SE cross section and the velocity scale is in the upper right corner of the figure.

a dense saline fluid (Maxworthy, 1983). In this experiment, Maxworthy observed solitary waves that propagated to the leading edge or nose of the gravity current where, apparently, the waves dissipated.

The previously presented evidence, although consistent with the premise that the thunderstorm generated the wave, does not preclude the converse premise. However, the fact that the earlier thunderstorm had no wave associated with it but, nevertheless, was of similar intensity and propagated along the same track, leads us to conclude that the mechanisms to sustain and steer the storms are identical and not related to the wave. Furthermore, the storm tracked to the NE at speeds of 23 m s^{-1}, whereas the wave propagated to the SE at 13 m s^{-1}. Yet, the wave remains connected to the southern flank of the storm. Observations suggest that the environment is homogeneous over the length of the wave, so there is no reason why one part of it would move at different speeds, unless the thunderstorm is generating the wave or unless the thunderstorm, controlled by mechanisms other than the wave, propagates coincidentally at a speed and direction that, apparently keep it attached to the wave. Finally, a plot of the time sequence of echo positions and extrapolation of the position of the wave backward in time beyond the horizon where it was first detected, leads to a conjunction of the storm and wave, again suggesting that the wave was generated by the storm.

On the other hand, waves may trigger thunderstorms. Purdom (1976) has shown several cases of satellite observations where propagating solitary disturbances appear to initiate thunderstorms, and the intersection of two disturbances is a favored location for storm initiation. It would be of great interest to know more about the dynamics of these disturbances and to determine whether they are related to solitary waves. Satellite data, combined with data from *in situ* measurements aboard aircraft, as well as remote measurements with Doppler radar and NASA's new airborne Doppler lidar (Bilbro *et al.*, 1984), would be extremely valuable in studying wave dynamics. Whereas Kelvin-Helmholtz waves have received close attention over the last two decades, larger mesoscale gravity and solitary waves are, as yet, inadequately observed and understood (Atkinson, 1981). Furthermore, we know very little about their role in momentum transfer and their possible effects on weather. But, in the next decade in which mesoscale meteorology may take a central position within the atmospheric sciences, further research can elucidate the relations between these waves, weather and hazards to aircraft.

In summary, examination of radar data (e.g., Fig. 1) suggests that the subject storm pulsated as a succession of cells fed into the right rear flank of the storm (or at least into the region of persistent high reflectivity). The storm produced a succession of downdrafts, and these formed a sequence of outflows which molded into a gravity current. The southeastward flowing gravity current penetrated a pycnocline established by an earlier storm and formed the solitary wave observed by tower and radar.

Acknowledgments. Our thanks to Michelle Foster for her accurate interpretation of the manuscript which tried her abilities and good humor. Joan Kimpel did the artwork. Robert Rabin gave much of his time and made valuable suggestions that are incorporated in this paper. We also give thanks to the team of engineers and technicians at the National Severe Storms Laboratory who are responsible for the

maintenance and operation of NSSL's facilities, without which the paper could not have been. Dr. D. R. Christie, of the Australian National University in Canberra, A.C.T., has made many valuable suggestions which have improved this paper. This work has been partially supported by the Federal Aviation Administration under Contract No. DTFA01-80-Y-10524.

REFERENCES

Atkinson, B. W., 1981: *Meso-scale Atmospheric Circulations.* Academic Press, 495 pp.

Beamer, C. M., 1970: Measured antenna beam cross-section contours on a 230-km tropospheric scatter circuit. Int. Rept., Collins Radio Company, Collins Comm. Res. Fac., Cedar Rapids, IA, 20 pp.

Bedard, A. J., Jr., F. H. Merrem, D. Simms and M. M. Cairns, 1979: A thunderstorm gust-front detection system. Part I—System operation and significant case studies. Part II—Statistical results. Rept. No. FAA-RD-79-55, August 1979, 130 pp.

Benjamin, T. B., 1967: Internal waves of permanent form in fluids of great depth. *J. Fluid Mech.,* **29,** 559–592.

Bilbro, J., G. Fichtl, D. Fitzjarrald, M. Krause and R. Lee, 1984: Airborne Doppler lidar wind-field measurements. *Bull. Amer. Meteor. Soc.,* **65,** 348–359.

Britter, R. E., and J. E. Simpson, 1981: A note on the structure of the head of an intrusive gravity current. *J. Fluid Mech.,* **112,** 459–466.

Christie, D. R., and K. J. Muirhead, 1982: Solitary waves: a hazard to aircraft operating at low altitudes. Report, Res. School of Earth Sci., Australian National University, 33 pp.

——, and ——, 1983a: Solitary waves: a hazard to aircraft operating at low altitudes. *Aust. Meteor. Mag.,* **31,** 97–109.

——, and ——, 1983b: Solitary waves: a low-level wind shear hazard to aviation. *Int. J. Aviat. Safety,* **1,** 169–190.

——, —— and A. L. Hales, 1978: On solitary waves in the atmosphere. *J. Atmos. Sci.,* **35,** 805–825.

——, —— and R. H. Clarke, 1981: Solitary waves in the lower atmosphere. *Nature,* **293,** 46–49.

Clarke, R. H., 1983: The morning glory. *Weatherwise,* **38,** 134–137.

——, R. K. Smith and D. G. Reid, 1981: The morning glory of the Gulf of Carpentaria: An atmospheric undular bore. *Mon. Wea. Rev.,* **109,** 1726–1750.

Doviak, R. J., D. Sirmans, D. Zrnic' and G. B. Walker, 1978: Considerations for pulse-Doppler radar observations of severe thunderstorms. *J. Appl. Meteor.,* **17,** 189–205.

Gossard, E. E., 1983: Aircraft hazard assessment from a clear-air radar and meteorological tower study of gravity wave events. June 1983, U.S. Dept. of Commerce, NOAA/ERL, U.S. Gov't. Printing Off., Washington DC, 20402, 18 pp.

Grimshaw, R., 1981: A second-order theory for solitary waves in deep fluids. *Phys. Fluids,* **24,** 1611–1618.

Haase, S., and R. K. Smith, 1984: Morning glory wave clouds in Oklahoma: A case study. *Mon. Wea. Rev.,* **112,** 2078–2089.

Hennington, L., 1981: Reducing the effects of Doppler radar ambiguities. *J. Appl. Meteor.,* **20,** 1543–1546.

Maxworthy, T., 1980: On the formation of nonlinear internal waves from the gravitational collapse of mixed regions in two and three dimensions. *J. Fluid Mech.,* **96,** 47–64.

——, 1983: Gravity currents with variable inflow. *J. Fluid Mech.,* **128,** 247–257.

Purdom, J. F. W., 1976: Some uses of high-resolution GOES imagery in the mesoscale forecasting of convection and its behavior. *Mon. Wea. Rev.,* **104,** 1474–1483.

Rust, W. D., and R. J. Doviak, 1982: Radar research on thunderstorms and lightning. *Nature,* **297,** 461–468.

Simpson, J. E., D. A. Mansfield and J. R. Milford, 1977: Inland penetration of sea-breeze fronts. *Quart. J. Roy. Meteor. Soc.,* **103,** 47–76.

Tung, K., D. R. S. Ko and J. J. Chang, 1981: Weakly nonlinear internal waves in shear. *Stud. Appl. Math.,* **65,** 189–221.

——, T. F. Chan and T. Kubota, 1982: Large amplitude internal waves of permanent form. *Stud. Appl. Math.,* **66,** 1–44.

Whitham, G. B., 1974: *Linear and Nonlinear Waves.* John Wiley & Sons, 636 pp.

Woodfield, A. A., 1983: Wind shear and vortex wake research in U.K. 1982. *Proc. Sixth Ann. Workshop Meteorological and Environmental Inputs to Aviation Systems,* W. Frost and D. W. Camp, Eds., NASA Rept. CP-2274 and Dept. of Transp. Rept. No. DOT/FAA/RD-82/72, 66–83.